AGU100 ADVANCING EARTH AND SPACE SCIENCE

Geophysical Research Letters

RESEARCH LETTER
10.1029/2018GL077875

Special Section:
Cassini's Final Year: Science Highlights and Discoveries

Auroral Hiss Emissions During Cassini's Grand Finale: Diverse Electrodynamic Interactions Between Saturn and Its Rings

A. H. Sulaiman[1], W. S. Kurth[1], G. B. Hospodarsky[1], T. F. Averkamp[1], A. M. Persoon[1], J. D. Menietti[1], S.-Y. Ye[1], D. A. Gurnett[1], D. Píša[2], W. M. Farrell[3], and M. K. Dougherty[4]

[1]Department of Physics and Astronomy, University of Iowa, Iowa City, Iowa, USA, [2]Institute of Atmospheric Physics CAS, Prague, Czech Republic, [3]NASA/Goddard Space Flight Center, Greenbelt, Maryland, USA, [4]Blackett Laboratory, Imperial College London, London, UK

Abstract The Cassini Grand Finale orbits offered a new view of Saturn and its environment owing to multiple highly inclined orbits with unprecedented proximity to the planet during closest approach. The Radio and Plasma Wave Science instrument detected striking signatures of plasma waves in the southern hemisphere. These all propagate in the whistler mode and are classified as (1) a filled funnel-shaped emission, commonly known as auroral hiss. Here however, our analysis indicates that they are likely associated with currents connected to the rings. (2) First observations of very low frequency saucers directly linked to the planet on field lines also connected to the rings. The latter observations are unique to low altitude orbits, and their presence at the Earth and Saturn alike shows that they are fundamental plasma waves in planetary ionospheres. Our results give an insight, from a unique perspective, into the dynamic and diverse nature of Saturn's environment.

Plain Language Summary Cassini's high-inclination Grand Finale orbits brought the spacecraft closer to Saturn than ever before, with the closest approach between the cloud tops and the inner edge of the D ring. This unprecedented set of orbits introduced a new view of Saturn's system by enabling direct measurements of the topside ionosphere as well as the rings' surrounding environment. Here we present evidence of communication between Saturn's ionosphere and rings via plasma waves. These results underline Saturn's system as one of the most dynamic and diverse in the solar system.

Key Points:
- Striking auroral hiss emissions are observed in Saturn's southern hemisphere
- Ray tracing analysis confirms that auroral hiss emissions originate from the rings
- We report the first observations of VLF saucers directly associated with Saturn's ionosphere

Correspondence to:
A. H. Sulaiman,
ali-sulaiman@uiowa.edu

Citation:
Sulaiman, A. H., Kurth, W. S., Hospodarsky, G. B., Averkamp, T. F., Persoon, A. M., Menietti, J. D., et al. (2018). Auroral hiss emissions during Cassini's Grand Finale: Diverse electrodynamic interactions between Saturn and its rings. *Geophysical Research Letters*, *45*, 6782–6789. https://doi.org/10.1029/2018GL077875

Received 9 MAR 2018
Accepted 13 APR 2018
Accepted article online 26 APR 2018
Published online 24 JUL 2018

1. Introduction

In September 2017, the Cassini spacecraft successfully completed its final phase, coined the "Grand Finale", which comprised a set of 22 highly inclined orbits and culminated in a deorbit by atmospheric entry. The kronographic equatorial crossings were at varying altitudes between the inner edge of the D ring and cloud tops, thus affording unprecedented proximity to the planet and directly sampling the topside ionosphere (Menietti et al., 2018; Persoon et al., 2018; Sulaiman et al., 2017; Wahlund et al., 2018). First results by Wahlund et al. (2018) revealed a cold, dense, and dynamic ionosphere with an electron density varying up to 2 orders of magnitude between orbits. Further, their results demonstrated a seasonally dependent north-south asymmetry in the upper ionospheric density.

The purpose of this letter is to report striking observations of whistler mode emissions detected by the Radio and Plasma Wave Science (RPWS) instrument (Gurnett et al., 2004) during Cassini's Grand Finale. This class of emissions is commonly referred to as auroral hiss, and although they are not always associated with the auroral regions, their nature and properties as the whistler mode are the same. Such emissions often exhibit characteristic funnel-shaped features in the electric field frequency-time spectrogram. Some of these emissions can manifest as "splashes" of V-shaped features and are reported here for the first time in direct association with the planet. The latter, called "saucers", have been detected at Earth and were typically found at low altitudes in the ionosphere (Ergun et al., 2003; James, 1976; Mosier & Gurnett, 1969). Segments of Cassini's trajectory during this final phase have been of the lowest altitudes, which includes Saturn's topside ionosphere, thus allowing for the detection of these features.

We present these two distinct kinds of whistler mode auroral-like processes in the southern hemisphere during some of the closest regions to Saturn. On electric field frequency-time spectrograms they are observed,

respectively, as (1) a filled funnel on time scales of minutes originating from multiple extended source regions in the rings and (2) "splashes" of V-shaped features on time scales of seconds originating from a cluster of discrete sources in the ionosphere. The latter are specifically called "saucers", in line with previous works cited in the text. Altogether, these emissions reveal the spatial extent of the ring's influences and provide a deeper insight into the Saturnian environment as one of the most dynamic and diverse in the solar system.

2. Auroral Hiss

The proximal orbits enabled close examination of the regions associated with the aurora as well as other active sites for electron beams such as near the rings and ionosphere. One of the most prominently observed magnetospheric emissions detected by an electric field instrument is auroral hiss. Auroral hiss propagates in the whistler mode with a lower frequency limit at the lower hybrid resonance frequency, f_{LH}, where the waves are reflected as their wave normal angles rotate through 90°. The allowable frequency range for the whistler mode to exist is below both electron cyclotron, f_{ce}, and electron plasma, f_{pe}, frequencies, with the theoretical upper cutoff at the lower of the two. They are thus trapped in planetary magnetospheres unlike, for example, the commonly observed Saturn kilometric radiation, which is a free space mode radio emission capable of being detected remotely (Zarka, 1998). Auroral hiss emissions have been extensively studied at Earth where they have often been observed to have a characteristic funnel shape on frequency-time spectrograms (Gurnett, 1966). Their source regions are understood to co-locate with auroral electron precipitation. Their spectral feature is attributed to a propagation effect such that the whistler mode's k-vector is restricted to a cone of angles with respect to the background magnetic field. For a given (angular) frequency, ω, the maximum wave normal angle is along the resonance cone, θ_{res}, where the refractive index, $n = ck/\omega$, approaches infinity and the whistler mode becomes quasi-electrostatic. Since the group velocity is defined as $\nabla_{\boldsymbol{k}}\omega(\boldsymbol{k})$, it follows that its vector is always perpendicular to the refractive index surface of constant ω. Hence, the wave energy's direction of travel is correspondingly limited, making an angle to the magnetic field as $\psi_{res} = 90° - \theta_{res}$.

For a strongly magnetized, low density plasma regime, that is, $f_{ce}^2 \gg f_{pe}^2$, descriptive of the region of interest during Cassini's Grand Finale, the angle ψ_{res} is given by

$$\tan^2 \psi_{res} = -\frac{S}{P} \simeq \frac{f^2}{f_{pe}^2 - f^2} \tag{1}$$

where S and P, as defined by Stix (1992), are elements of the dielectric tensor for waves in a cold plasma. By virtue of the frequency dependence, higher frequencies propagate at larger angles with respect to the local magnetic field, thereby being detected farther from the source magnetic field line compared to lower frequencies. This property leads to the funnel or V-shaped feature on spectrograms (Gurnett et al., 1983).

At Jupiter and Saturn alike, these funnel shapes have been observed repeatedly, though not all on field lines threading high-latitude auroral source regions. Nevertheless, the fundamental processes driving these waves are believed to the same. During the early stage of the Cassini mission, Xin et al. (2006) performed ray-tracing calculations on a whistler mode emission and found the source to be close to Saturn's B ring. Kopf et al. (2010) analyzed low-frequency whistler mode emissions and concluded that the generation mechanism is linked to electron beams, similar to its terrestrial counterpart. Gurnett et al. (2011) and Leisner et al. (2013) reported auroral-like processes near Enceladus, revealing an electrodynamic interaction between the icy moon and Saturn's magnetosphere. Furthermore, Sulaiman et al. (2018) reported observations of auroral hiss emissions near Saturn's ionosphere on a flux tube connected to Enceladus. Auroral hiss has also been recently observed in Jupiter's high latitude regions by the Juno spacecraft in its similar orbit to Cassini's final phase (Tetrick et al., 2017). Altogether, these reports, among many others, underline both the ubiquity and diversity of auroral hiss emissions in planetary magnetospheres.

3. Observations

We use high-resolution data from the electric field-measuring component of the RPWS instrument, provided by the wideband receiver (WBR). The frequency upper limit was either 10.5 or 75 kHz, depending on the mode. The spectral resolution was typically 13.6 Hz for the former mode and 109 Hz for the latter mode.

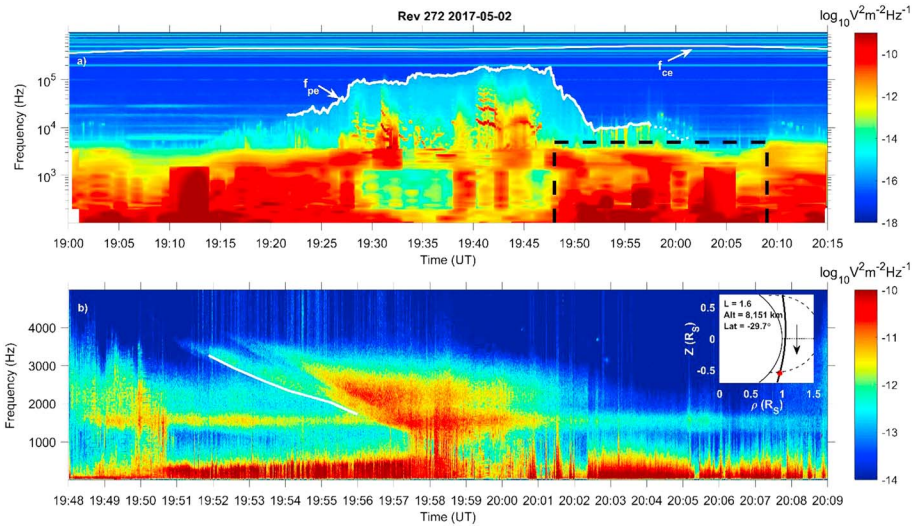

Figure 1. (a) Low rate electric field dynamic spectrogram taken on 2 May 2017. The electron cyclotron frequency is measured directly by the fluxgate magnetometer and represented by the top solid white line labeled f_{ce}. The electron plasma frequency is the upper cutoff of the broadband hiss emission and represented by the bottom solid white line labeled f_{pe}, as identified by Persoon et al. (2018). The dashed white lines are where the upper cutoff is not so clear. (b) High rate electric field dynamic spectrogram from the wideband receiver taken during the interval delimited by the dashed black box in (a). The orbital trajectory is illustrated in the inset figure. The red spot represents the apex position of the above funnel-shaped emission at ~19:58. The black arrow represents the direction of Cassini's travel. The white solid line in (b) is the range of frequencies used in ray-tracing analysis (see Figure 4).

The temporal resolution was typically 125 ms/spectrum. A five-channel waveform receiver provided coarse electric and magnetic field power spectra up to a frequency of 2.5 kHz. This ensemble allowed for distinguishing between electrostatic and electromagnetic emissions. More details on the RPWS instrument, particularly a schematic of the triaxial electric antennae arrangement, can be found in Gurnett et al. (2004).

Figure 1a shows a low-rate frequency-time spectrogram of the electric field during orbit 272 between 19:00 and 20:15 on 2 May 2017. Overlaid is the electron cyclotron frequency, f_{ce}, which is derived from direct measurements using Cassini's onboard fluxgate magnetometer (Dougherty et al., 2004) and given by f_{ce} [Hz] = 28 $|\boldsymbol{B}|$ [nT]. The broadband continuum (light blue) is observed repeatedly during the Grand Finale when Cassini was in the ionosphere and is interpreted as a whistler mode emission. Since the upper cutoff is well below the f_{ce} line, it is therefore identified as f_{pe}, and this agrees well with independently measured electron densities by Cassini's Langmuir probe (Persoon et al., 2018; Wahlund et al., 2018), thus satisfying the relationship f_{pe} [Hz] = 8980 $\sqrt{n_e}$ [cm^{-3}]. The densities measured during the southern outbound passes were consistently lower than those of the northern inbound passes for a specific range of latitudes, and this has been attributed to ring shadowing effects during northern summer solstice (Hadid, Morooka, Wahlund, Moore, et al., 2018). Figure 1b shows the WBR high-rate data in the interval 19:48 to 20:09 (dashed box in Figure 1a), depicting a classic example of a filled funnel-shaped emission. The apex point at 19:58 UT was observed from an altitude of 8,151 km, latitude of −29.7°, L shell of 1.6, and local time 14.02, as shown by the inset figure. Here it appears that the funnel may not be propagating all the way up to f_{pe}, as the broadband continuum suggests (see Figure 1a), and possible reasons for this are expanded upon in the next section. The Langmuir probe does not provide reliable densities for this particular orbit as it is exposed to the spacecraft wake. This filled funnel-shaped emission is not the only one observed during the Grand Finale orbits. At lower latitudes, filled funnels are observed symmetrically north and south of the equator from orbit to orbit, and we reserve the statistical study of these for a separate work. We focus here on the aforementioned single event as it is both seemingly unique and isolated from those filled funnels observed repeatedly between orbits.

The emissions from Figure 1b were inspected for possible magnetic signatures in tandem with the enhancement in electric field power. Figure 2 displays components from the five-channel waveform receiver. Panels 1

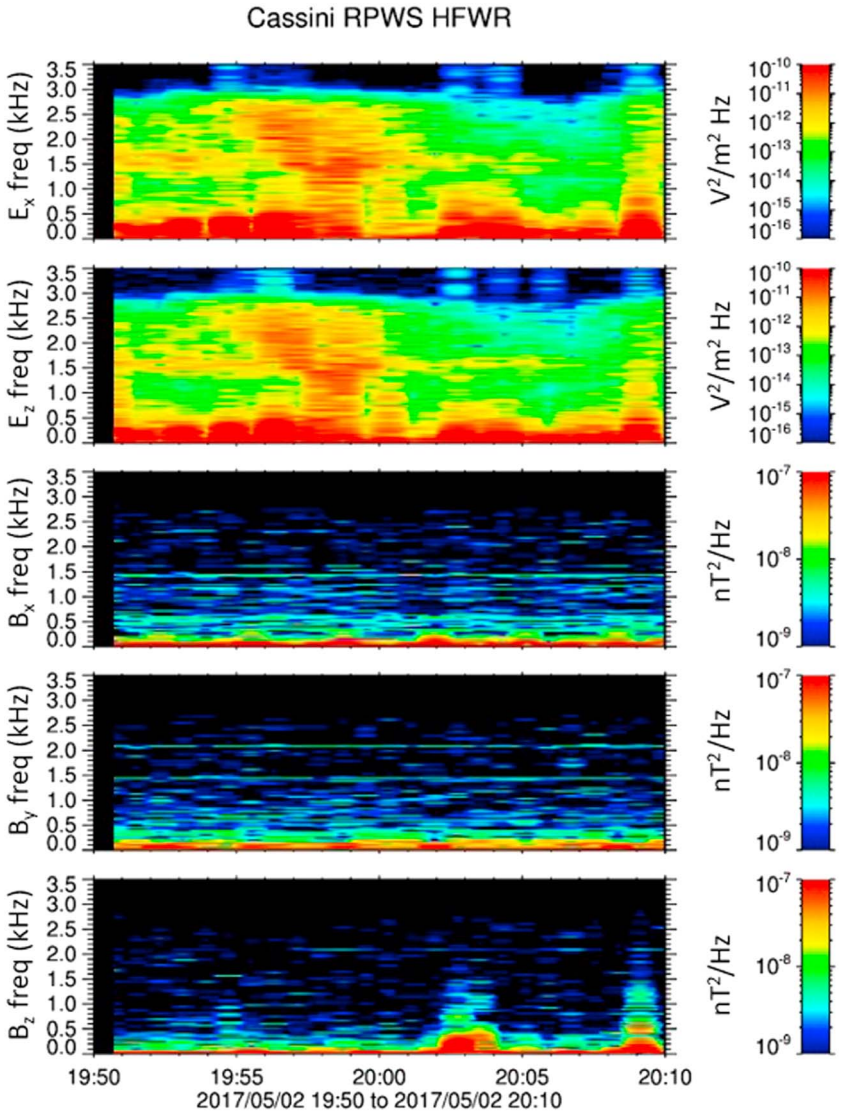

Figure 2. Same emission as Figure 1b recorded by the five-channel waveform receiver. (top rows) E_X and E_Z and (bottom rows) B_X, B_Y, and B_Z.

and 2 are spectrograms of two components of the electric field (E_x and E_z, parallel to the corresponding spacecraft axes), and panels 3–5 are the three components of the magnetic field as measured by the triaxial search coils. The absence of a magnetic signature indicates the electrostatic nature of the whistler mode emissions and therefore propagation along the resonance cone. There are, on the other hand, a few electromagnetic signatures in the whistler mode at ~20:03 and ~20:09, though these are limited to much lower frequencies and are most likely separate from the emission of interest. The absence of appreciable power in the magnetic field means it is not possible to calculate the Poynting vector. Nevertheless, with the knowledge that the emission is propagating along the resonance cone, equation (1) can be used to perform a ray-tracing analysis and identify the possible source region.

Figures 3a and 3b are WBR electric field spectrograms of two VLF saucers, similar to those detected during low altitude passes at Earth (Ergun et al., 2003). These are detected in the southern hemisphere at a lower L shell of 1.2–1.3 and a lower altitude of ~5,000 km as shown by their corresponding inset figures. f_{LH} is overlaid on both, and in this highly magnetized regime, it is approximately the proton plasma frequency (Sulaiman et al., 2017).

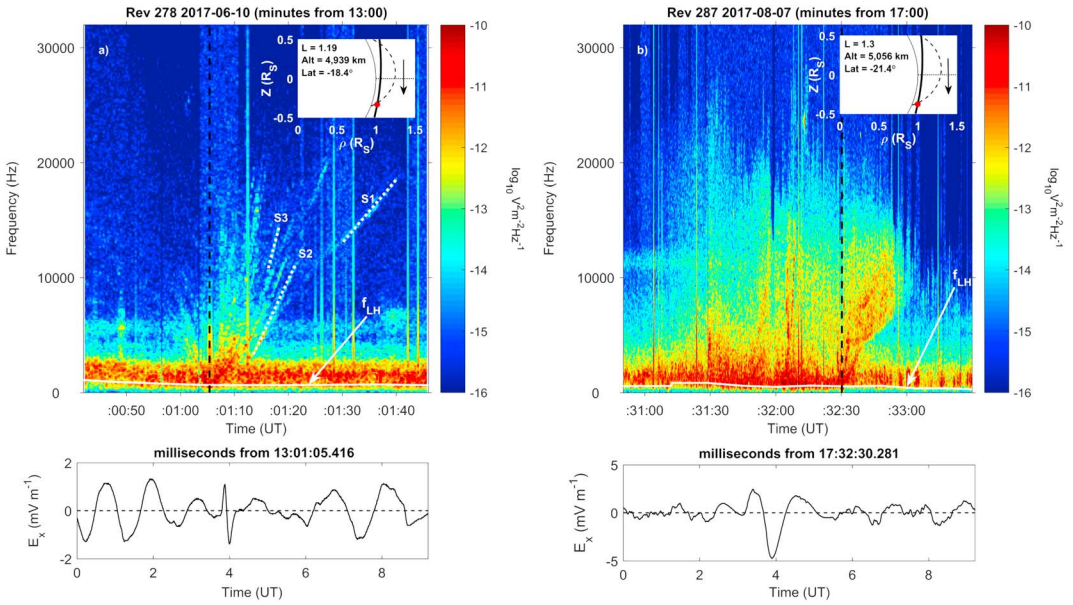

Figure 3. (a) High rate electric field spectrogram of very low frequency saucer on 10 June 2017. The lower hybrid frequency is represented by the white solid line. The orbital trajectory is illustrated in the inset figure, and the red spot represents the location at time represented by the black dashed line in the spectrogram. The black arrow represents the direction of Cassini's travel. The panel below is a waveform time series during time represented by the black dashed line. (b) Similar emission detected on 7 August 2017.

4. Discussion

4.1. Filled Funnel Emission

A distinct feature of the whistler mode emission visible in Figure 1b is the presence of a double funnel (or more, though not as unambiguous). This patchwork is likely due to multiple adjacent extended sources of finite distances apart. Each extended source launches whistler mode waves along the resonance cone (as Figure 2 confirms their electrostatic nature) and entirely fills a funnel feature. By digitizing the inbound side of the outer funnel emission (solid white line on Figure 1b), we are able to compute its possible paths from ray-tracing analysis. In this highly magnetized regime, as shown by equation (1), the angle of propagation is principally dependent on f_{pe}. Therefore, an ionospheric model describing the density variation with respect to altitude in the southern hemisphere is required for our analysis (Figure 4b from Persoon et al., 2018). We have used their simple two-part exponential fit to averaged data, and this is given by $n_e = 58{,}620e^{(-h/575)} + 135e^{(-h/2360)}$, where n_e is the electron number density in cm^{-3} and h is the altitude in km. Detailed interpretation of the scale heights is discussed in Persoon et al. (2018). We accounted for the error bars (one standard deviation above and below the mean) by comparing different coefficients and found no significant changes to the source location. Figure 4 illustrates the location, collapsed into ρ-Z space, of the whistler mode emission along Cassini's trajectory with two convergence possibilities of the raypath: directions parallel and antiparallel to the background magnetic field. Since we cannot differentiate between upward and downward propagating waves in the absence of a Poynting vector, one of the two possibilities cannot be categorically ruled out.

Figure 4a shows the range of frequencies converging to the D ring which has a width spanning 1.11–1.24 R_s (1 R_s = 60,268 km; Saturn's equatorial radius), as labeled. Similarly, the frequencies corresponding to the inner funnel yield very similar results (not shown here), and its source is only a small distance shifted toward the planet. Figure 4b, on the other hand, shows convergence toward the planet. Ideally, the frequencies should converge to a point coinciding with the location of the source region. The main factor responsible for the lack of point convergence is the dependence of the ray-tracing to the ionospheric model. Large variability is embedded in the averaged power laws used, which are not perfectly representative of the density in this particular orbit. Further, at larger distances from the source, the error associated with computing its exact

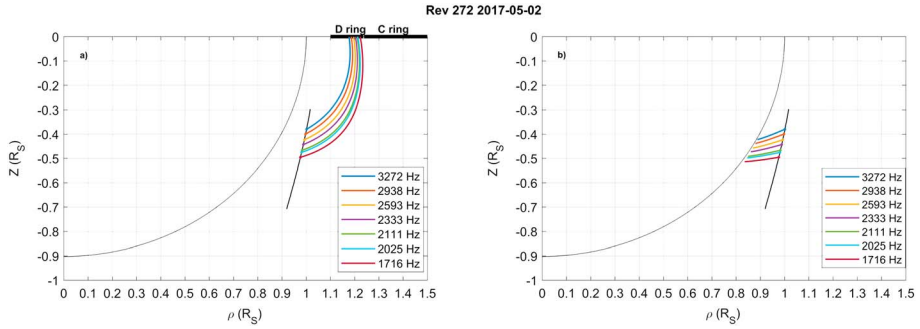

Figure 4. Ray-tracing analysis performed on event in Figure 1b with the waves assumed to start their journey toward a direction (a) parallel and (b) antiparallel to the source magnetic field. Coordinate system is the Saturn Solar Equatorial with X defined in the planet-Sun plane and positive toward the Sun, Z defined as the northward spin axis of Saturn, $Y = Z \times X$, and $\rho = \sqrt{(X^2 + Y^2)}$.

position becomes larger. There are reasons why Figure 4a is the more likely picture. First, the emission does not propagate all the way up to the local f_{pe}, as shown in Figure 1. It may be generated at an alternative active site of lower electron density than the ionosphere, that is, near the rings. Therefore, the remote sources near the rings launch whistler waves with frequencies up to the lower f_{pe} at the site and are detected by the spacecraft at a region of higher f_{pe} near the ionosphere. The progressively higher density toward the planet means that these frequencies can propagate unhindered. Second, electrodynamic coupling to the rings has been demonstrated by observations of auroral hiss-like emissions originating from near the B rings (Gurnett et al., 2005; Xin et al., 2006). Third, given the closer distance to the supposed source in Figure 4b, the frequencies should show markedly better convergence. Finally, we note a scenario where Figures 4a and 4b are not necessarily mutually exclusive events. Maggs (1989) interpreted funnel shapes as being formed when downgoing auroral hiss is reflected at the ionosphere boundary when $f = f_{LH}$. The reflected upgoing emissions then propagate along the resonance cone and amplify waves. We therefore propose that the rings are the more likely and realistic possibility for the source of this emission, whether or not they are reflected back at the ionosphere. Furthermore, employing the ionospheric model for the northern hemisphere, which is larger by an order of magnitude for a given altitude, does not yield convergence. Thus, we conclude that the location at the rings is of reasonable accuracy and the D ring is the planetward limit of extended and multiple source regions.

4.2. VLF Saucers

The VLF saucers in Figure 3, similarly, are believed to arise from the same propagation effect as the filled funnels since they are both in the whistler mode. However, whereas the filled funnels are understood to originate from extended sources, the saucers are associated with discrete point sources that are highly localized in both longitude and latitude to the spacecraft. Indeed, Figure 5 shows frequencies (labeled S2 on Figure 3a) converging to a point toward the ionosphere at distance of ~1,000 km below the spacecraft.

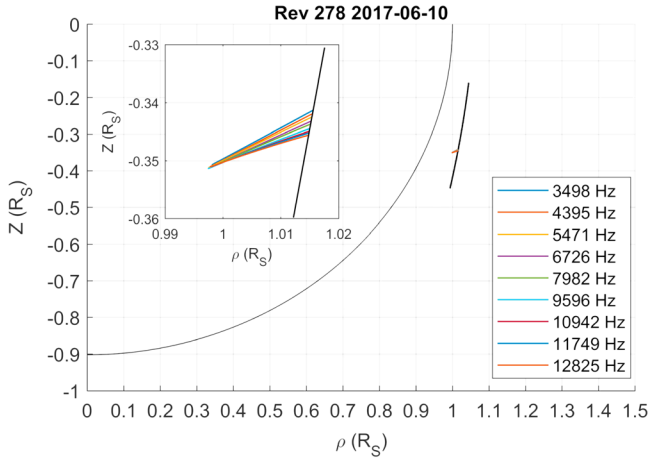

Figure 5. Ray-tracing analysis performed on the emission labeled S2 in Figure 3a.

At Earth, Ergun et al. (2001) analyzed two saucers detected by the FAST satellite and interpreted their "arms" as evidence for multiple discrete sources along the field lines below the spacecraft. They estimated their distances to be 100–700 km from the spacecraft. Employing the formalism by Ergun et al. (2003) as an alternative means to ray-tracing, we are capable of making an estimation of Cassini's distance from the saucers. This approximate distance, d, can be expressed as

$$d \simeq \frac{v_{sat} f_{pe}}{\frac{df}{dt}} \tag{2}$$

where v_{sat} denotes the spacecraft speed and df/dt the slope of an arm on the frequency-time spectrogram. For the arms of different slopes labeled S1–S3 on Figure 3a, the distances were ~500–1,700 km, in very

good agreement with the ray-tracing method. Moreover, the apices of the saucers are broadly consistent with the local f_{LH} for both cases, which suggests small longitudinal or lateral offsets. A quantitative comparison of distances can be made if the outer boundary of the filled funnel in Figure 1b is considered an arm. This would translate to a distance of ~70,000–100,000 km (i.e., $>1\ R_S$), depending on lower and upper limits of f_{pe}. While the comparison is rudimentary and the quantities are unlikely to be reflective of the exact distances, it remains instructive from an order-of-magnitude perspective. Note that the saucer events occur over much shorter time scales compared to the filled funnel, hence the larger slopes of their arms, which are inversely proportional to their distances.

The mechanism generating auroral hiss emissions typically requires the presence of electron beams as the source of energy. Saturn's rings are known to be a prime environment for radial currents by virtue of a differential azimuthal motion between ring particles and the corotating magnetospheric plasma. Planetward of the synchronous point, that is, where their speeds are exactly matched, the ring particles are traveling at Keplerian speed, faster than the corotating plasma. This results in an effective drag force between the two populations that is balanced by a $\boldsymbol{J} \times \boldsymbol{B}$ force. The current responsible is the radial current along the ring plane that is directed planetward. The reverse is true for the region antiplanetward of the synchronous orbit. Somewhere along the rings, current closure occurs along paths of least resistance, that is, magnetic field lines, as electron beams which complete the loops in the ionosphere (see Figure 8 from Xin et al., 2006). This model is at least one picture of the large-scale current system in Saturn's magnetosphere. The filled funnels would require an electron beam from the rings, that is, an upward current from Saturn's southern ionosphere to the rings. The reverse would be true for the saucers. Since they are localized, they must be generated from upgoing electrons, that is, downward current in Saturn's southern ionosphere from the rings. Indeed, James (1976) and Ergun et al. (2003) found the majority of saucers to be generated on flux tubes carrying antiearthward (upgoing) electrons in the downward current region of the aurora. Given the low latitudes of the saucers detected at Saturn (~−20°), they are probably not linked to the aurora but instead return currents connected to the rings. Furthermore, the apices of the saucers are coincident with bipolar and tripolar electrostatic solitary structures as shown in the bottom panels of Figure 3. These are associated with electron phase-space holes typically observed with saucers (Ergun et al., 2001). Finally, the fact that these emissions presented here are not repeatedly detected with every orbit suggests that the currents are probably not highly structured but rather dynamic. It is worth mentioning that the events presented here were all detected in the southern hemisphere. This may be due to asymmetric current systems caused by seasonal effects. Indeed, Hadid, Morooka, Wahlund, Persoon, et al. (2018) found more pronounced ring-planet electrodynamic interactions in the southern hemisphere during the Grand Finale orbits. Future results by the magnetometer instrument onboard Cassini will shed light on the large-scale current system at Saturn, particularly during the Grand Finale orbits.

5. Summary and Conclusion

We have presented observations of auroral-like processes in regions closest to Saturn exclusively made possible by the Grand Finale orbits. These emissions propagate in the whistler mode, and two classes have been analyzed with the conclusions as follows: (1) the filled funnel emission propagating along the resonance cone and originating from multiple extended sources located in a region of lower electron density, that is, the rings, and (2) first observations of VLF saucers associated with the planet, originating from discrete sources close to the spacecraft. Observing them at Earth and Saturn, which have vastly different magnetospheric systems, shows that VLF saucers are fundamental emissions in planetary ionospheres. Altogether, these results highlight the diversity of plasma waves present at Saturn and the dynamic and complex interactions the planet has with its environment.

Acknowledgments
Useful discussions with O. Santolík and D. G. Mitchell are gratefully acknowledged. Cassini RPWS data will be publicly available via NASA's Planetary Data System on a project-agreed schedule. Prior to this, the data may be requested from the lead author. The research at the University of Iowa was supported by NASA through contract 1415150 with the Jet Propulsion Laboratory. D. P. acknowledges the support from grant 16-16050Y of the Grant Agency of the Czech Republic.

References

Dougherty, M. K., Kellock, S., Southwood, D. J., Balogh, A., Smith, E. J., Tsurutani, B. T., et al. (2004). The Cassini magnetic field investigation. *Space Science Reviews*, *114*(1-4), 331–383. https://doi.org/10.1007/s11214-004-1432-2

Ergun, R. E., Carlson, C. W., McFadden, J. P., Strangeway, R. J., Goldman, M. V., & Newman, D. L. (2001). Electron phase-space holes and the VLF saucer source region. *Geophysical Research Letters*, *28*(19), 3805–3808. https://doi.org/10.1029/2001GL013024

Ergun, R. E., Carlson, C. W., McFadden, J. P., Strangeway, R. J., Goldman, M. V., & Newman, D. L. (2003). Fast auroral snapshot satellite observations of very low frequency saucers. *Physics of Plasmas*, *10*(2), 454–462. https://doi.org/10.1063/1.1530160

Gurnett, D. A. (1966). A satellite study of VLF hiss. *Journal of Geophysical Research*, *71*(23), 5599–5615. https://doi.org/10.1029/JZ071i023p05599

Gurnett, D. A., Shawhan, S. D., & Shaw, R. R. (1983). Auroral hiss, Z mode radiation, and auroral kilometric radiation in the polar magnetosphere: DE 1 observations. *Journal of Geophysical Research*, *88*(A1), 329–340. https://doi.org/10.1029/JA088iA01p00329

Gurnett, D. A., Averkamp, T. F., Schippers, P., Persoon, A. M., Hospodarsky, G. B., Leisner, J. S., et al. (2011). Auroral hiss, electron beams and standing Alfvén wave currents near Saturn's moon Enceladus. *Geophysical Research Letters*, *38*, L06102. https://doi.org/10.1029/2011GL046854

Gurnett, D. A., Kurth, W. S., Hospodarsky, G. B., Persoon, A. M., Averkamp, T. F., Cecconi, B., et al. (2005). Radio and plasma wave observations at Saturn from Cassini's approach and first orbit. *Science*, *307*(5713), 1255–1259. https://doi.org/10.1126/science.1105356

Gurnett, D. A., Kurth, W. S., Kirchner, D. L., Hospodarsky, G. B., Averkamp, T. F., Zarka, P., et al. (2004). The Cassini radio and plasma wave investigation. *Space Science Reviews*, *114*(1-4), 395–463. https://doi.org/10.1007/s11214-004-1434-0

Hadid, L. Z., Morooka, M. W., Wahlund, J.-E., Moore, L., Cravens, T. E., Hedman, M. M., et al. (2018). Ring shadowing effects on Saturn's ionosphere: Implications for ring opacity and plasma transport. *Geophysical Research Letters*, https://doi.org/10.1029/2018GL079150

Hadid, L. Z., Morooka, M. W., Wahlund, J.-E., Persoon, A. M., Andrews, D. J., Shebanits, O., et al. (2018). Saturn's ionosphere: Electron density altitude profiles and D-ring interaction from the Cassini Grand Finale. *Geophysical Research Letters*, https://doi.org/10.1029/2018GL078004

James, H. G. (1976). VLF saucers. *Journal of Geophysical Research*, *81*(4), 501–514. https://doi.org/10.1029/JA081i004p00501

Kopf, A. J., Gurnett, D. A., Menietti, J. D., Schippers, P., Arridge, C. S., Hospodarsky, G. B., et al. (2010). Electron beams as the source of whistler mode auroral hiss at Saturn. *Geophysical Research Letters*, *37*(9), L09102. https://doi.org/10.1029/2010GL042980

Leisner, J. S., Hospodarsky, G. B., & Gurnett, D. A. (2013). Enceladus auroral hiss observations: Implications for electron beam locations. *Journal of Geophysical Research*, *118*(1), 160–166. https://doi.org/10.1029/2012JA018213

Maggs, J. E. (1989). Nonlinear evolution of the auroral electron beam. *Journal of Geophysical Research*, *94*(A4), 3631. https://doi.org/10.1029/JA094iA04p03631

Menietti, J. D., Averkamp, T. F., Ye, S.-Y., Sulaiman, A. H., Morooka, M. W., Persoon, A. M., et al. (2018). Analysis of intense Z-mode emission observed during the Cassini proximal orbits. *Geophysical Research Letters*, *45*. https://doi.org/10.1002/2018GL077354

Mosier, S. R., & Gurnett, D. A. (1969). VLF measurements of the Poynting flux along the geomagnetic field with the Injun 5 satellite. *Journal of Geophysical Research*, *74*(24), 5675–5687. https://doi.org/10.1029/JA074i024p05675

Persoon, A. M., Kurth, W. S., Gurnett, D. A., Groene, J. B., Sulaiman, A. H., Wahlund, J.-E., et al. (2018). Electron density distributions in Saturn's ionosphere. *Geophysical Research Letters*, https://doi.org/10.1029/2018GL078020

Stix, T. H. (1992). *Waves in plasmas*. New York: American Institute of Physics.

Sulaiman, A. H., Kurth, W. S., Persoon, A. M., Menietti, J. D., Farrell, W. M., Ye, S. Y., et al. (2017). Intense harmonic emissions observed in Saturn's ionosphere. *Geophysical Research Letters*, *44*, 12,049–12,056. https://doi.org/10.1002/2017GL076184

Sulaiman, A. H., Kurth, W. S., Hospodarsky, G. B., Averkamp, T. F., Ye, S.-Y., Menietti, J. D., et al. (2018). Enceladus auroral hiss emissions during Cassini's Grand Finale. *Geophysical Research Letters*, https://doi.org/10.1029/2018GL078130

Tetrick, S. S., Gurnett, D. A., Kurth, W. S., Imai, M., Hospodarsky, G. B., Bolton, S. J., et al. (2017). Plasma waves in Jupiter's high-latitude regions: Observations from the Juno spacecraft. *Geophysical Research Letters*, *44*, 4447–4454. https://doi.org/10.1002/2017GL073073

Wahlund, J.-E., Morooka, M. W., Hadid, L. Z., Persoon, A. M., Farrell, W. M., Gurnett, D. A., et al. (2018). In situ measurements of Saturn's ionosphere show that it is dynamic and interacts with the rings. *Science*, *359*(6371), 66–68. https://doi.org/10.1126/science.aao4134

Xin, L., Gurnett, D. A., Santolík, O., Kurth, W. S., & Hospodarsky, G. B. (2006). Whistler-mode auroral hiss emissions observed near Saturn's B ring. *Journal of Geophysical Research*, *111*, A06214. https://doi.org/10.1029/2005JA011432

Zarka, P. (1998). Auroral radio emissions at the outer planets: Observations and theories. *Journal of Geophysical Research*, *103*(E9), 20,159–20,194. https://doi.org/10.1029/98JE01323